

EXPERIMENTAL STUDY OF MULTIPLE-SHOT UNITARY CHANNELS DISCRIMINATION USING THE IBM Q COMPUTERS

ADAM BÍLEK^{1,2}, JAN HLISNIKOVSKÝ^{*,1,2}, TOMÁŠ BEZDĚK¹, RYSZARD KUKULSKI²,
AND PAULINA LEWANDOWSKA²

1. ABSTRACT

Tasks involving black boxes appear frequently in quantum computer science. An example that has been deeply studied is quantum channel discrimination. In this work, we study the discrimination between two quantum unitary channels in the multiple-shot scenario. We challenge the theoretical results concerning the probability of correct discrimination with the results collected from experiments performed on the IBM Quantum processor Brisbane. Our analysis shows that neither too deep quantum circuits nor circuits that create too much entanglement are suitable for the discrimination task. We conclude that circuit architectures which minimize entanglement overhead while preserving discrimination power are significantly more resilient to hardware noise if their depth does not overpass threshold value.

2. INTRODUCTION

In the last decade, quantum computing has become a reality. Quantum algorithms of increasing degree of complexity are currently being implemented on more and more complex quantum devices. In effect, high-quality solutions to some real-world problems are expected to be forthcoming soon. This situation motivates the need for the certification and benchmarking of various quantum devices [1, 2, 3]. The discrimination task of quantum operators constitutes one of the certification methods and quality metrics for benchmarking quantum architectures [4]. The theoretical background of the quantum discrimination task has been widely developed. The primary task of discrimination involves a one-shot scenario of discrimination between quantum operators. We can imagine that we have an unknown quantum device, a black-box. The only information we have is that it performs one of two quantum operators, say \mathcal{T} and \mathcal{S} . Our goal is two-fold. First, we want to determine the highest possible probability of correct guessing. Secondly, we need to devise an optimal strategy that maximizes the probability of success.

¹ DEPARTMENT OF APPLIED MATHEMATICS, FACULTY OF ELECTRICAL ENGINEERING AND COMPUTER SCIENCE, VSB-TECHNICAL UNIVERSITY OF OSTRAVA, 17. LISTOPADU 2172/15, 708 33 OSTRAVA, CZECH REPUBLIC

²IT4INNOVATIONS, VSB - TECHNICAL UNIVERSITY OF OSTRAVA, 17. LISTOPADU 2172/15, 708 33 OSTRAVA, CZECH REPUBLIC

* CORRESPONDING AUTHOR. E-MAIL: jan.hlisnikovsky@live.com

The problem of single-shot discrimination of quantum states was solved analytically by Helstrom a few decades ago in [5, 6]. The authors have calculated the probability of correct discrimination between two quantum states using the notion of a trace norm. Next, there are many modifications of the origin problem for quantum states that were also considered [7, 8, 9, 10, 11]. For the discrimination tasks of the quantum channels [6], the probability of success of the discrimination can be formulated by the diamond norm [12, 13], which can be computed by semidefinite programming [14, 12]. However, for increasing the dimension of quantum channels in the diamond norm, the size of the problem does not allow efficient computation [15]. In general, for general quantum channels, entanglement is necessary for optimal discrimination [6]. The exception is, for example, the discrimination task between unitary channels [6, 16]. Furthermore, the probability of correct discrimination between two unitary channels can be expressed in the notion of the numerical range [17]. The discrimination tasks for general quantum measurements, von Neumann measurements, or SIC POVMs were also considered in the literature [18, 19, 20, 21, 22, 23]. Lastly, the theory of an indefinite causal structure is one of the attractive topics. This approach uses the notion of process matrices [24, 25], which can be seen as a generalization of quantum combs. The single-shot discrimination of the process matrices was introduced [26].

What if we have multiple copies of quantum operators? The most general discrimination approach is known as adaptive strategy [27]. This strategy can be described by using the term quantum combs. Here, we assume freedom in choosing the setting of quantum operations and any processing between them. In addition, numerical investigation of quantum channel discrimination showed that using indefinite causal order, we can achieve greater success discrimination [28, 29]. However, determining an optimal strategy to realize such tasks is a significant challenge in practice. This is why we often limit ourselves to parallel [30] and sequential [31] schemes. The parallel scheme assumes N copies of a given quantum operation distributed over N entangled systems and final measurement with no additional processing, whereas the sequential scheme assumes the implementation of N copies of the quantum operation on one system, allowing additional processing between them.

One of the first theoretical results was the study of discrimination of multipartite unitary operations [28]. The authors were shown that perfect discrimination can be achieved using a parallel scheme [30]. Simultaneously, it is also possible to create a perfect discrimination scheme of unitary channels without creating the entanglement with the auxiliary system [32]. It can be done by using the sequential approach and specific processing at the end of the circuit. On the other hand, for general quantum channels, neither parallel nor sequential strategy guarantees optimal solutions [33, 34]. The advantage of adaptive strategies became apparent for a task concerning entanglement-breaking channels [33]. The discrimination tasks in which adaptive scenarios were also investigated in [31], [35, 21]. In the work [36], the authors have formulated the necessary and sufficient conditions under which quantum channels can be perfectly discriminated, while in [21], the authors have formulated conditions for the perfect discrimination of two measurements. Furthermore, in [37], the authors have shown that any possible adaptive method does not offer any advantage over the parallel scheme for von Neumann measurements.

One of the first experimental results for the parallel and sequential discrimination scheme of unitary channels was presented [38]. In the era of NISQ devices, we need to take into

account certain limitations. Due to the existing decoherence, sequential schemes could not be practical for larger numbers of copies. At the same time, parallel schemes for NISQ architectures are also not possible to implement because of the limited number of qubits. Perhaps intermediate schemes called sequentially-paralleled will prove to solve both of these obstacles. This scheme assumes that we have $N = w \cdot d$, copies of a quantum operator, where k and l are natural numbers. The sequentially-paralleled scheme of width w and depth d consists of d applications of w copies of the quantum operator applied simultaneously to the quantum state. The initial state ρ evolves through these layers, combining parallelism within each layer and a sequential structure across layers. In general, one could consider incorporating additional intermediate processing operations between layers.

In this work, we present a comprehensive study of various scenarios of multiple-shot discrimination of quantum unitary channels. We consider parallel, sequential, and sequentially-paralleled quantum networks for discrimination between two qubit unitary channels. We challenge the theoretical results concerning the probability of correct discrimination with the results collected from experiments performed on the IBM Quantum processor Brisbane. Based on several examples, the analysis shows that neither too deep quantum circuits nor circuits that create too much entanglement are suitable for the discrimination task.

This paper is organized as follows. Section 3 presents the necessary mathematical preliminaries. Section 4 introduces the task of discriminating quantum channels in single and multiple-shot scenarios. Sections 5 and 6 are dedicated examples of quantum unitary channel discrimination performed on NISQ devices. Finally, Section 7 summarizes the main contributions and results of this work.

3. MATHEMATICAL PRELIMINARIES

Let \mathcal{X} be a complex Euclidean space, then $L(\mathcal{X})$ denotes the collection of all linear mappings of the form $A : \mathcal{X} \rightarrow \mathcal{X}$. An operator $X \in L(\mathcal{X})$ is positive semi-definite if $\langle x | X | x \rangle \geq 0$ for all $|x\rangle \in \mathcal{X}$. The set of all such operators is written as $\text{Pos}(\mathcal{X})$. By $\Omega(\mathcal{X})$ we denote the set of quantum states $\rho \in \text{Pos}(\mathcal{X})$ such that $\text{Tr}\rho = 1$. Let $X \in L(\mathcal{X})$, by $\text{spec}(X)$ we express the set of all eigenvalues of X .

The set of all linear mappings from $L(\mathcal{X})$ into $L(\mathcal{Y})$, $\Phi : L(\mathcal{X}) \rightarrow L(\mathcal{Y})$, will be denoted as $T(\mathcal{X}, \mathcal{Y})$. A linear map $\Phi \in T(\mathcal{X}, \mathcal{Y})$ is positive if holds $\Phi(P) \in \text{Pos}(\mathcal{Y})$ for all $P \in \text{Pos}(\mathcal{X})$, whereas Φ is a completely positive map (CP) if $\Phi \otimes \mathbb{1}_{L(\mathcal{Z})}$ is a positive map for every complex Euclidean space \mathcal{Z} . We say Φ is trace-preserving (TP) if it holds that $\text{Tr}(\Phi(X)) = \text{Tr}(X)$ for all $X \in L(\mathcal{X})$. A linear map $\Phi \in T(\mathcal{X}, \mathcal{Y})$, which is a CPTP map, is called a quantum channel. The collection of all quantum channels is denoted as $C(\mathcal{X}, \mathcal{Y})$ (with a shortcut $C(\mathcal{X}) := C(\mathcal{X}, \mathcal{X})$). Next, we distinguish a special subset of quantum channels known as unitary channels, $\Phi_U \in C(\mathcal{X})$ defined as $\Phi_U(X) = UXU^\dagger$ where $U \in L(\mathcal{X})$ is the unitary matrix.

A Positive Operator-Valued Measure (POVM) \mathcal{P} is a collection of operators, the so-called effects $\{E_0, \dots, E_n\} \subset \text{Pos}(\mathcal{X})$ with the property of $\sum_{i=0}^n E_i = \mathbb{1}$. According to the Born rule for a given quantum state ρ the probability of obtaining the result E_i is given by $\text{Tr}(E_i\rho)$.

An useful tool for studying the discrimination of unitary channels is the concept of the numerical range of an operator. For $X \in L(\mathcal{X})$ we define the numerical range of X as the set

$$W(X) := \{\langle x|X|x\rangle : |x\rangle \in \mathcal{X}, \langle x|x\rangle = 1\}. \quad (1)$$

The Hausdorff-Töplitz Theorem [39, 40] states that $W(X)$ is a convex set. If X is normal, the numerical range is a convex hull of its eigenvalues. For unitary matrices U we define the arc function $\theta(U)$ as the length of the smallest arc on the unit circle that contains all the eigenvalues of the unitary operator U . Mathematically, this can be expressed as

$$\theta(U) := \min \left\{ \Delta \in [0, 2\pi) : \exists \alpha \in [0, 2\pi) \text{ such that } \right. \\ \left. \text{spec}(U) \subset \{e^{i\theta} : \theta \in [\alpha, \alpha + \Delta]\} \right\}. \quad (2)$$

Lastly, let us introduce the diamond norm in the space $T(\mathcal{X}, \mathcal{Y})$. For $\Phi \in T(\mathcal{X}, \mathcal{Y})$ it is defined as

$$\|\Phi\|_{\diamond} = \|\Phi \otimes \mathbb{1}_{L(\mathcal{X})}\|_1, \quad (3)$$

where $\|\Phi\|_1 = \max\{\|\Phi(X)\|_1 : X \in L(\mathcal{X}), \|X\|_1 \leq 1\}$ and $\|Y\|_1$ is Schatten 1-norm of $Y \in L(\mathcal{Y})$.

4. DISCRIMINATION OF QUANTUM CHANNELS

We will consider the following scenario of quantum channel discrimination. Suppose that we have a classical description of two quantum channels, $\Phi_0, \Phi_1 \in C(\mathcal{X}, \mathcal{Y})$ and a black box containing a quantum channel Φ , which is either Φ_0 or Φ_1 . We would like to determine whether $\Phi = \Phi_0$ or $\Phi = \Phi_1$ have been hidden in the black box. To reveal the value of Φ we can construct a quantum experiment which will consist of an initial state $\rho \in \Omega(\mathcal{X} \otimes \mathcal{Z})$ and a binary measurement $\{E_0, E_1\} \subset \text{Pos}(\mathcal{Y} \otimes \mathcal{Z})$. The channel $\Phi \otimes \mathbb{1}_{L(\mathcal{Z})}$ is applied on ρ and then the output state $(\Phi \otimes \mathbb{1}_{L(\mathcal{Z})})(\rho)$ is measured by $\{E_0, E_1\}$. The measurement label defines our guess about the hidden value of Φ (the label 0 associated with the effect E_0 indicates $\Phi = \Phi_0$). In such setup, the probability p_{succ} of successful channel discrimination is given as

$$p_{\text{succ}} = \frac{1}{2} \text{Tr}(E_0(\Phi_0 \otimes \mathbb{1}_{L(\mathcal{Z})})(\rho)) + \frac{1}{2} \text{Tr}(E_1(\Phi_1 \otimes \mathbb{1}_{L(\mathcal{Z})})(\rho)). \quad (4)$$

The goal of our task is to construct ρ and $\{E_0, E_1\}$ that maximize p_{succ} . The auxiliary system \mathcal{Z} is of arbitrary size and provides a resource to increase the probability of success. From the Holevo-Helstrom theorem [41, 5] we know the probability of successful channel discrimination can be expressed by the help of the diamond norm

$$p_{\text{succ}} = \frac{1}{2} + \frac{1}{4} \|\Phi_0 - \Phi_1\|_{\diamond}. \quad (5)$$

4.1. Single-shot discrimination of quantum unitary channels. Considering the task of discrimination between unitary channels Φ_U, Φ_V , the diamond norm between such channels can be expressed using the notion of the numerical range as [42, 43]

$$\|\Phi_U - \Phi_V\|_\diamond = 2\sqrt{1 - \nu^2}, \quad (6)$$

where $\nu = \min_{w \in W(V^\dagger U)} |w|$. From the above proposition it follows that unitary channels Φ_U and Φ_V are perfectly distinguishable if and only if $0 \in W(V^\dagger U)$. The above can also be formulated as there exists a density matrix σ , such that $\text{tr}(V^\dagger U \sigma) = 0$.

Using the results of [44, 45, 32] we can calculate ν using the arc function $\theta(V^\dagger U)$, determining the condition for perfect discrimination between U and V in single-shot scenario. We achieve perfect discrimination if and only if

$$\theta(V^\dagger U) \geq \pi. \quad (7)$$

This condition ensures that zero lies in the numerical range of $V^\dagger U$. Hence, an input state can be chosen such that it evolves under Φ_U to a state that is orthogonal to the same input state evolved under Φ_V .

4.2. Multiple-shot discrimination of unitary channels. When multiple uses of the unitary channel are available, perfect discrimination may be achieved even if the single-shot condition $\theta(V^\dagger U) \geq \pi$ is not met [44]. The theoretically best strategy in that case is a parallel scheme which consists of N copies of the unitary U applied simultaneously to N quantum registers. In that case, the problem is to discriminate identity $U^{\otimes N}$ and unitary matrix $V^{\otimes N}$. Since the arc function satisfies the scaling relation $\theta((V^{\otimes N})^\dagger U^{\otimes N}) = N\theta(V^\dagger U)$, for $N\theta(V^\dagger U) < 2\pi$, then the condition for perfect discrimination is $N\theta(V^\dagger U) \geq \pi$ [32]. This leads to the condition on the minimum number of copies required for perfect discrimination is given by

$$N \geq \left\lceil \frac{\pi}{\theta(V^\dagger U)} \right\rceil. \quad (8)$$

Thus, even when $\theta(V^\dagger U) < \pi$, as long as $\theta(V^\dagger U) > 0$, perfect discrimination can still be achieved by using a sufficient number of copies of U and V .

4.3. Experimental set-up. A wide range of multi-shot discrimination strategies have been explored in the literature. In this work, we restrict our attention to three representative classes: parallel schemes, sequential schemes, and rectangular hybrid schemes that interpolate between these two. Experimental comparison of the performance of these strategies will constitute the contribution of our work. Our attention is put on the discrimination of qubit unitary channels U and V . For simplicity we will consider only the cases that satisfy

$$\theta(V^\dagger U) = \frac{\pi}{N}. \quad (9)$$

Let $N = wd$ for $w, d \in \mathbb{N}$. In our set-up N copies of the black box Φ can be composed in the rectangular shape spread on w qubits with the depth of the circuit d . On each qubit the unknown operation is composed d times, namely we have

$$\Phi^{\otimes w} \circ \Phi_{X_{d-1}} \circ \Phi^{\otimes w} \circ \dots \circ \Phi_{X_1} \circ \Phi^{\otimes w}, \quad (10)$$

where X_1, \dots, X_{d-1} are arbitrary unitary matrices defined on w qubits which are responsible for mid-circuit processing. In special cases, when $w = N$ and $d = 1$ we have the parallel scheme $\Phi^{\otimes N}$ (no processing is needed) and when $w = 1$ and $d = N$ we have the sequential scheme $\Phi \Phi_{X_{d-1}} \dots \Phi_{X_1} \Phi$.

In general, for $d > 1$ if we do not apply mid-circuit processing ($X_i = \mathbb{1}$) then theoretically the scheme will be strictly worse than the parallel scheme ($d = 1$). For example, comparing sequential scheme without processing ($d = N$) and parallel scheme, we get $\theta((V^N)^\dagger U^N) < \theta((V^{\otimes N})^\dagger U^{\otimes N}) = \pi$ for most (with respect to the Haar measure) pairs of U, V . However, if we choose a simple processing $X_i = (V^\dagger)^{\otimes w}$ we get

$$\theta(((V^\dagger U)^d)^{\otimes w}) = w\theta((V^\dagger U)^d) = wd\theta(V^\dagger U) = N\frac{\pi}{N} = \pi. \quad (11)$$

This means that for all w, d satisfying $wd = N$ we achieve perfect discrimination for all N -shot scenarios we consider. Hence, in theory, all three scenarios: parallel, sequential, and hybrid are equal and give $p_{\text{succ}} = 1$.

The only remaining question is how to find optimal ρ and $\{E_0, E_1\}$? The precise form of these variables depends on U, V and will be calculated later for each pair of unitary channels considered. It is worth sympathizing at this point that there is no need to use an auxiliary system \mathcal{Z} for the discrimination of quantum unitary channels [29].

5. DISCRIMINATION OF UNITARY CHANNELS ON IBM-Q WITH NO PROCESSING

This section is divided into four main parts. At the beginning, we will discuss in details the components of discrimination schemes, and later on their decompositions into native gates. Next, we will talk about transpilation approaches, and finally we will present the results obtained from the IBM Q device. All experiments were executed on the IBM Quantum processor Brisbane.

5.1. Example 1. In this example, we will distinguish between identity $\Phi_{\mathbf{1}}$ and $\Phi_{\text{RZ}(\phi)}$ for $\text{RZ}(\phi) = \begin{pmatrix} e^{-i\frac{\phi}{2}} & 0 \\ 0 & e^{i\frac{\phi}{2}} \end{pmatrix}$ without processing between the particular application of the unitary channel ($X_i = \mathbb{1}$ for each $i = 1, \dots, d$). Let $N = wd$ for $w, d \in \mathbb{N}$. In our setup N copies of the black box Φ can be composed in the rectangular shape spread on w qubits with the depth of the circuit d . On each qubit the unknown operation is composed d times, so namely we have

$$\underbrace{\Phi^d \otimes \dots \otimes \Phi^d}_w. \quad (12)$$

To determine a discriminator $|\psi\rangle$, we need to find a unit vector satisfying

$$\langle \psi | \text{RZ}(d\phi)^{\otimes w} | \psi \rangle = 0. \quad (13)$$

The most distant pair of eigenvalues of $\text{RZ}(d\phi)^{\otimes w}$ are $-i, i$ corresponding to eigenvectors $|0 \dots 0\rangle, |1 \dots 1\rangle$, respectively. Hence, we can show that

$$|\psi\rangle = \frac{1}{\sqrt{2}} (|0 \dots 0\rangle + \lambda |1 \dots 1\rangle) \in \mathbb{C}^{2^w}, \quad (14)$$

for any unit number $\lambda \in \mathbb{C}$. If $\Phi = \Phi_{\mathbf{1}}$, the output state is equal to $|\psi_0\rangle = |\psi\rangle$. Otherwise, if $\Phi = \Phi_{\text{RZ}(\phi)}$, then the output states are equal to $|\psi_1\rangle = \text{RZ}(d\phi)^{\otimes w} |\psi\rangle = \frac{-i}{\sqrt{2}} (|0 \cdots 0\rangle - \lambda |1 \cdots 1\rangle)$. As $|\psi_0\rangle$ and $|\psi_1\rangle$ are orthogonal, we can find $E_0 \geq |\psi_0\rangle\langle\psi_0|$ and $E_1 \geq |\psi_1\rangle\langle\psi_1|$ (in particular $E_0 = |\psi_0\rangle\langle\psi_0|$ and $E_1 = \mathbb{1} - E_0$), which in summary will guarantee $p_{\text{succ}} = \frac{1}{2} \text{Tr}(E_0(\Phi_{\mathbf{1}^{\otimes w}}(|\psi\rangle\langle\psi|))) + \frac{1}{2} \text{Tr}(E_1(\Phi_{\text{RZ}(d\phi)^{\otimes w}}(|\psi\rangle\langle\psi|))) = \frac{1}{2} \text{Tr}(E_0 |\psi_0\rangle\langle\psi_0|) + \frac{1}{2} \text{Tr}(E_1 |\psi_1\rangle\langle\psi_1|) = 1$.

5.2. Components of the discrimination scheme and decompositions. We divided the implementation of our discrimination circuit into two distinct components: the discriminator and the measurement. The unknown unitary gates, representing the quantum channel to be identified, are inserted between these two parts. In practical experiments, we focus specifically on schemes that in theory achieve perfect discrimination between the identity operation and the $\text{RZ}(\phi)$ gate. To ensure that the condition previously discussed is met, we set the angle ϕ to π/N , where N denotes the total number of uses of the unknown gate in the circuit. This value is determined by the product of the width (the number of qubits used in parallel) and depth (the number of successive applications of the unknown gate).

After the usage of the discriminator, the circuit has to be in a maximal entangled state, on N qubits in the form

$$|\psi\rangle = \frac{1}{\sqrt{2}} \left(|0\rangle^{\otimes N} + \alpha |1\rangle^{\otimes N} \right). \quad (15)$$

To achieve this, we used a cascade of CNOT gates, as can be seen for six qubits in Fig. 1. This discriminator is created based on the obvious pattern that is commonly used to create the GHZ state [46].

We run our experiments on IBM Brisbane, where the CNOT gate is not a native gate. To reduce the number of gates in the circuit, we prepare the discriminator specially designed for Eagle R3 architecture [47]. Then, we use ECR gates to create entanglement between qubits, omitting unrolling of CNOT gates during transpilation at the same time. The first part of the discriminator consists of SX gates on all qubits and then a cascade of ECR gates of similar structure as the CNOT cascade in the first case. Unlike the discriminator based on CNOT gates, we also had to add several X gates to the end of the discriminator to get the desired quantum state. There is little to no pattern in the qubits on which the X gate has to be applied. Therefore, we had to prepare the discriminator for each number of qubits separately by hand. In Fig. 2, we see the decomposition of ECR gate on six qubits. As we could see, in this case the X gates are applied on second and third qubits.

Two distinct methods were used to implement a circuit representing the measurement. The first method, referred to as the short measurement approach, is characterized by a reduced circuit depth and overall gate count. However, this advantage is offset by an increased susceptibility to bit-flip errors. This circuit could be implemented using CNOT gates, presented in Fig. 3, or ECR gates, as in Fig. 5. For the CNOT-based implementation, the measurement outcomes exhibit a regular structure: the scheme for the identity channel consistently yields the all-zero bitstring, while for the unitary channel $\Phi_{\text{RZ}(\theta)}$ produces bitstrings that are zero in all positions except for a single qubit set to one. The second measurement approach is different; it is much deeper, but the result for the identity

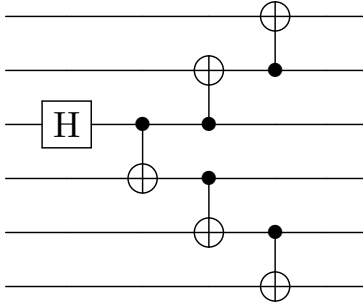


FIGURE 1. CNOT implementation of the discriminator.

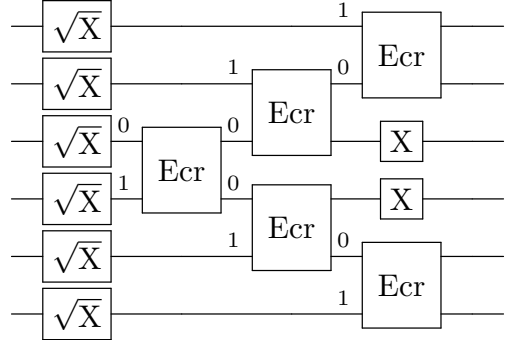


FIGURE 2. ECR implementation of the discriminator.

channel consists of all zeros, and the result for the unitary channel consists of all ones. This enables omitting several bit flip errors; we take a measured result, and if the majority of bits have value zero, we take it as the result of all zeros. In the case of a six-qubit system, and in the absence of noise, the observed bitstrings are 000000 for identity and 001000 for the unitary channel $\Phi_{\text{RZ}(\theta)}$.

In contrast, the ECR-based implementation returns a more complex distribution of output bitstrings, lacking the clear structure observed in the CNOT-based case. With this implementation, we get two disjoint subsets of all possible results, one subset for identity and the second subset for the unitary channel $\Phi_{\text{RZ}(\theta)}$. For our example on six-qubit system, we obtain the following two sets of bitstrings after measurement: $\{001111, 010111, 101101, 110101, 100001, 100111, 011101, 110011, 000011, 111001, 011011, 111111, 001001, 000101, 010001, 101011\}$ for the identity channel and $\{110001, 001011, 011111, 100011, 001101, 110111, 000001, 010101, 000111, 101001, 111101, 010011, 101111, 111011, 011001, 100101\}$ for $\Phi_{\text{RZ}(\frac{\pi}{6})}$. The bitstring 001111 from the first set and 001101 from the second differ by only one bit, which may be problematic in a noisy environment. Even in this small example, we could see that processing these results is not so straightforward but is compensated for by the simplicity of the measurement circuit.

In both measurement schemes, if it is not possible to determine which channel was applied during experiment, i.e., when the distance to both candidate channels is equal, then the output is assigned randomly via a coin flip. This approach ensures that each circuit run yields a definite outcome, thereby avoiding missing data points. Analogically, if the majority of bits have value one, we take this as the result of all of them.

The ECR gates are oriented, so we cannot swap qubits that are being acted on by ECR. This fact causes that simple mapping logical to physical qubits on IBM Eagle R3 [47], without transpilation of our ECR discriminator and measurement, is possible just for circuits not bigger than few qubits. For discrimination tasks for higher dimensions, we have two possible solutions. For slightly bigger circuits, we are able to manually rearrange the

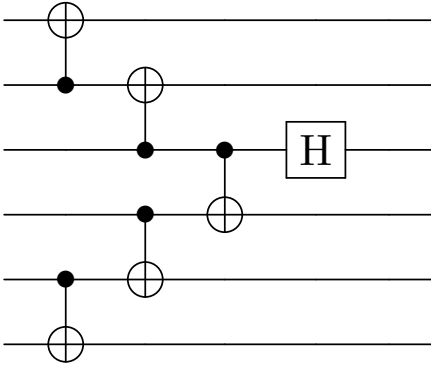


FIGURE 3. CNOT implementation of the short measurement.

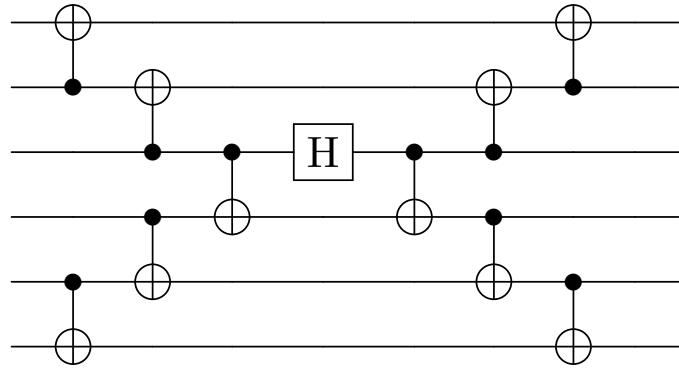


FIGURE 4. CNOT implementation of the XOR measurement.

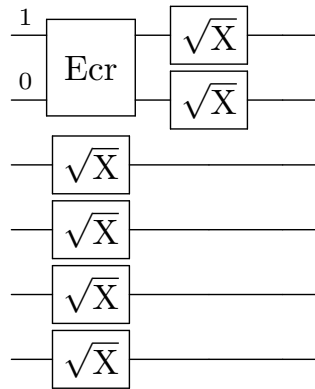


FIGURE 5. ECR implementation of the short measurement.

circuit, but it has to be done specifically for every number of qubits. The second possibility is to use swap gates. This enables relatively easy mapping of the circuits, but it enlarges the depth of the circuits.

5.3. Comparative analysis of transpilation. To evaluate the efficacy of different quantum circuit transpilation approaches, particularly concerning the choice between CNOT and ECR gates and the impact of manual qubit mapping, experiments were conducted on the 6-qubit and the 11-qubit systems. The objective is to compare the performance, measured by result accuracy, for circuits utilizing either the short measurement or the

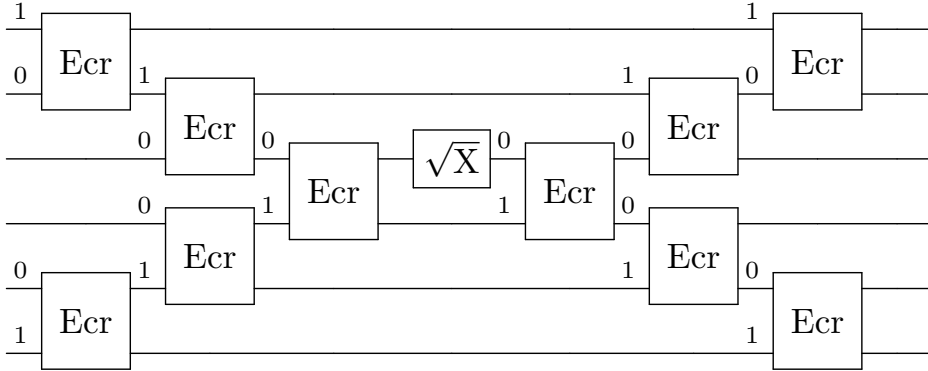


FIGURE 6. ECR implementation of the XOR measurement.

XOR-based measurement scheme, while varying the transpilation method. In all these cases, a pure parallel discrimination scheme was employed.

5.3.1. *6-qubit system evaluation.* For the 6-qubit configuration, four distinct transpilation strategies were evaluated for the short measurement and XOR-based measurement protocols:

- (1) **CNOT + Transpiler:** Circuit implemented using CNOT basis gates, processed by the Qiskit transpiler with optimization level 3.
- (2) **ECR + Transpiler:** Circuit implemented using ECR basis gates, processed by the Qiskit transpiler with optimization level 3.
- (3) **ECR + Transpiler + Fixed Mapping:** Circuit implemented using ECR basis gates, processed by the Qiskit transpiler with optimization level 3 and a predetermined, fixed mapping of logical qubits to physical qubits.
- (4) **ECR + Fixed Mapping (No Opt.):** Circuit implemented using ECR gates, utilizing a fixed logical-to-physical qubit mapping, bypassing subsequent transpiler optimization passes.

The experimental results, summarized in Table 1, indicate that for this system size, applying a fixed qubit mapping does not yield a discernible improvement in accuracy compared to relying solely on the transpiler’s default ECR implementation. This observation is potentially attributable to the limited circuit depth and complexity inherent in six-qubit systems, where the transpiler’s optimization might already find near-optimal solutions without explicit mapping constraints.

5.3.2. *11-qubit system evaluation.* A subsequent set of experiments was performed using the 11-qubit system. Five transpilation strategies were assessed for each measurement type:

- (1) **CNOT + Transpiler:** Circuit using CNOT basis gates, transpiled with optimization level 3.

Transpilation Strategy	Measurement	
	Short	XOR
CNOT + Transpiler	88.8%	86.4%
ECR + Transpiler	83.8%	90.0%
ECR + Transpiler + Fixed Map	84.4%	85.3%
ECR + Fixed Map (No Opt.)	83.3%	85.6%

TABLE 1. Accuracy of different transpilation strategies for discrimination scheme on 6-qubit obtained on IBM Brisbane, using short and XOR measurement schemes. Each circuit was executed with 10,000 shots. Ambiguous measurement outcomes were randomly assigned.

- (2) **ECR + Transpiler:** Circuit using ECR basis gates, transpiled with optimization level 3.
- (3) **ECR (Topology-Aware) + Transpiler:** Circuit initially designed considering device connectivity using ECR gates, then transpiled with optimization level 3.
- (4) **ECR (Topology-Aware) + Transpiler + Fixed Mapping:** Topology-aware ECR circuit, transpiled with optimization level 3 and a fixed logical-to-physical qubit mapping.
- (5) **ECR (Topology-Aware) + Fixed Mapping (No Opt.):** Topology-aware ECR circuit with fixed mapping, bypassing subsequent transpiler optimization.

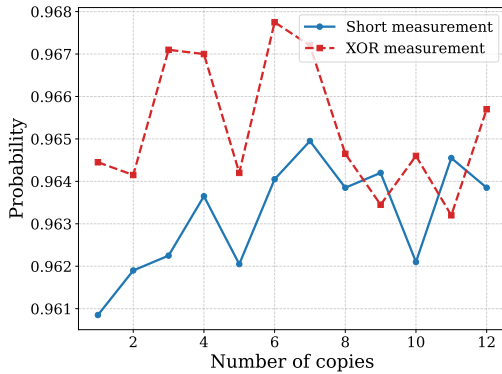
As detailed in Table 2, the results for the 11-qubit system demonstrate a general performance advantage for ECR-based implementations over CNOT-based ones for both measurement protocols. For the short measurement scheme, the standard ECR implementation processed by the transpiler (Method 2) yields the highest accuracy (55.0%). However, a more pronounced effect is observed for the XOR measurement protocol. Employing a topology-aware circuit design combined with fixed qubit mapping (Methods 4 and 5) results in a significant accuracy improvement, achieving approximately 71.5%–71.8%, nearly a 20% absolute increase compared to the standard CNOT transpiled approach (48.5%).

Transpilation Strategy	Measurement	
	Short	XOR
CNOT + Transpiler	43.3%	48.5%
ECR + Transpiler	55.0%	54.5%
ECR (Topol.) + Transpiler	36.1%	47.2%
ECR (Topol.) + Transpiler + Fixed Map	32.0%	71.5%
ECR (Topol.) + Fixed Map (No Opt.)	33.4%	71.8%

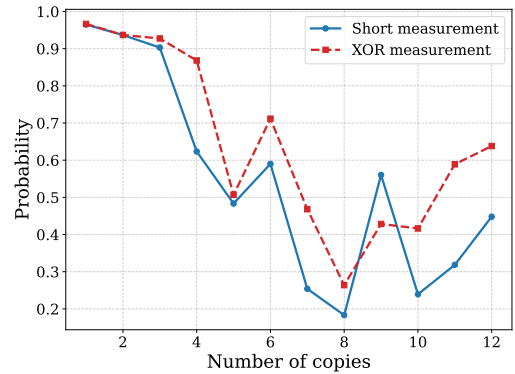
TABLE 2. Accuracy of different transpilation strategies for discrimination scheme on 11-qubit obtained from on IBM Brisbane using short and XOR measurement schemes. Each circuit was executed with 10,000 shots. Ambiguous measurement outcomes were randomly assigned.

It is worth observing that the substantial accuracy gain observed for the 11-qubit XOR measurement using hardware-aware design and fixed mapping highlights the potential benefits of tailoring circuits to specific device characteristics. However, this approach presents a significant practical challenge: it currently necessitates manual, device-specific, and qubit-count-specific circuit construction and mapping. This process lacks straightforward algorithmic automation and requires considerable expert intervention for each target configuration, limiting its scalability and general applicability.

5.4. Results. From the initial experiments involving purely sequential and purely parallel discrimination schemes (see Fig. 7), we observe that the use of entangling gates on real quantum devices introduces a greater error overhead than the decoherence effects arising from increased gate depth in sequential protocols. To further investigate this observation,



(a) Purely sequential scheme of discrimination.



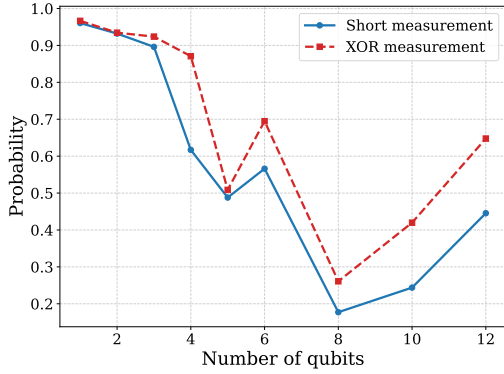
(b) Purely parallel scheme of discrimination.

FIGURE 7. Probability of successful discrimination between the identity operation and the $RZ(\pi/N)$ gate, where N is number of copies of unknown unitary. The dashed red line corresponds to the XOR-based measurement strategy, while the solid blue line represents the short measurement scheme. Figure (a) illustrates the performance of the purely sequential scheme, and Figure (b) corresponds to the purely parallel scheme. Each circuit was executed with 10,000 shots per gate. Measurement outcomes that could not be unambiguously associated with either gate were randomly assigned to one of the two possible answers.

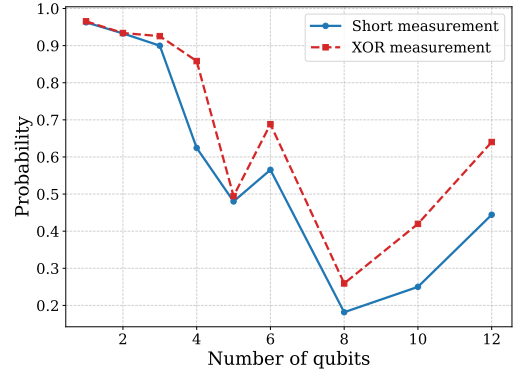
we conducted a series of tests using hybrid rectangular (sequentially-parallel) schemes with a fixed number of unknown gate applications (see Fig. 8). The results consistently show a significant increase in error rates as more entangling gates are introduced. This trend reinforces the conclusion that the primary source of performance degradation in current devices stems from the imperfections of multi-qubit gate operations rather than decoherence from circuit depth alone. Another notable observation is that different measurement

schemes have a visible but not dominant impact on the overall error rate, further suggesting that the circuit width and the number of entangled qubits are the primary contributors to performance degradation. This reinforces the conclusion that the main source of error arises from the entanglement rather than from the specifics of the measurement strategy.

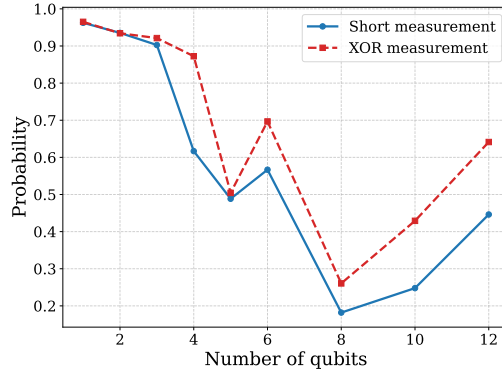
5.5. Discussion. During the experiments, we identified a specific issue with the IBM Q platform namely measurements in experiments involving entanglement of specific number, typically five or more, qubits exhibited random bit-flip errors. This type of error is evident in Fig. 7 and Fig. 8 and appears to affect the measurement results of all qubits at the same time independent of the measurement strategy. In particular, these anomalies can be removed simply by swapping the sets of expected answers, effectively compensating for the observed flips and restoring consistency in the results. To ensure that the issue was not caused by errors in our own implementation, we performed several verification steps. First, the experiments were repeated multiple times on different dates. Second, the final transpiled circuits were simulated using a noiseless simulator to confirm the expected theoretical behavior. Third, we applied M3 error mitigation techniques, which had no effect on overall results. Given that the observed errors persist across all experiments, regardless of the RZ gate angle or the measurement strategy employed, we hypothesize the presence of a systematic hardware or software artifact specific to the IBMQ platform, particularly the Brisbane quantum device. Further investigation and hypothesis-driven testing are required to understand this behavior.



(a) Hybrid scheme for $N = 120$.

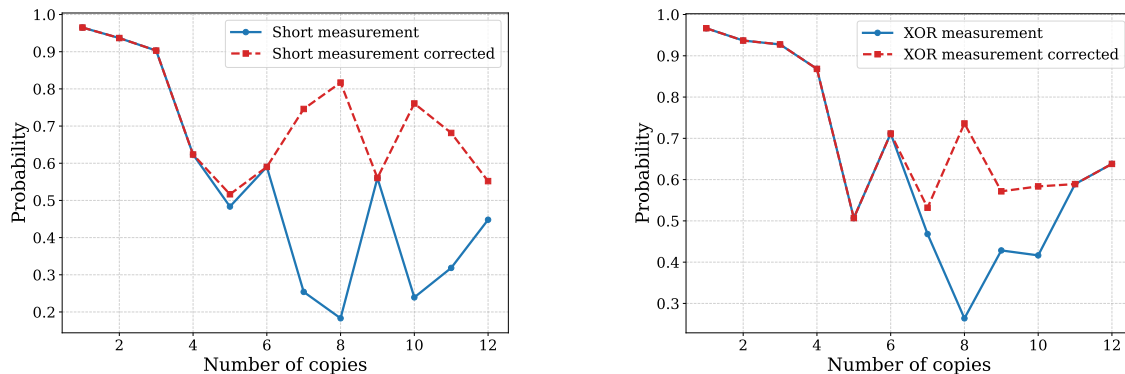


(b) Hybrid scheme for $N = 240$.



(c) Hybrid scheme for $N = 1200$.

FIGURE 8. Probability of successful discrimination between the identity operation and the $RZ(\pi/N)$ gate, where N is number of copies of unknown unitary as a function of the width of hybrid rectangular scheme. The dashed red line corresponds to the XOR-based measurement strategy, while the solid blue line represents the short measurement scheme. Figure (a) illustrates the performance of hybrid scheme with 120 copies in total, Figure (b) corresponds to hybrid scheme with 240 copies in total, and Figure (c) corresponds to hybrid scheme with 1200 copies in total. Each circuit was executed with 10,000 shots per gate. Measurement outcomes that could not be unambiguously associated with either gate were randomly assigned to one of the two possible answers.



(a) Usage of the short measurement.

(b) Usage of the XOR measurement.

FIGURE 9. Probability of successful discrimination between the identity gate and the $\text{RZ}(\pi/N)$ gate, where N is number of copies of unknown unitary as a function of the number of channel uses in purely parallel scheme, after applying post-processing correction. The dashed red line corresponds to the corrected measurement strategy, where the sets of answers associated with each channel were swapped in cases where the success probability dropped below 0.5. The solid blue line shows the original results using the short measurement strategy. Figure (a) presents the performance of the short measurement scheme, while Figure (b) displays the XOR-based scheme. Each circuit was executed with 10,000 shots per gate. Measurement outcomes that could not be unambiguously attributed to either gate were randomly assigned to one of the two possible answers.

6. DISCRIMINATION OF UNITARY CHANNELS ON IBM-Q WITH PROCESSING

In this section, we will present the second example of discrimination task with a different pair of unitary channels and run it on IBM Quantum processor Brisbane.

6.1. Example 2. In the second experiment, we take the following unitary channels to discriminate Φ_U for $U = \sqrt{X}\text{RZ}(\frac{-\pi}{2N})\sqrt{X}$ and Φ_V for $V = \sqrt{X}\text{RZ}(\frac{\pi}{2N})\sqrt{X}$, where $\sqrt{X} = \frac{1}{2} \begin{pmatrix} 1+i & 1-i \\ 1-i & 1+i \end{pmatrix}$. It is easy to check that condition $\theta(V^\dagger U) = \frac{\pi}{N}$ is satisfied. It implies that for N -shot discrimination scenario, we will achieve perfect discrimination. Let us fix $N = wd$, where $w, d \in \mathbb{N}$. In this setup, instead of mid-processing $X_i = (V^\dagger)^{\otimes w}$ we use hardware-friendly processing $X_i = X^{\otimes w}$. For convince we add also pre-processing unitary operation $X_0 = (X\sqrt{X})^{\otimes w}$ and post-processing operation $X_d = (\sqrt{X}X)^{\otimes w}$. Combining processing operators with the black-box Φ_U we get the following unitary operation

$$U_* = X_d U^{\otimes w} X_{d-1} \cdots X_1 U^{\otimes w} X_0 = \left(\text{RZ}\left(\frac{-\pi}{2N}\right)^d \right)^{\otimes w}. \quad (16)$$

Similarly, for Φ_V the combined unitary circuit equals $V_* = (\text{RZ}(\frac{\pi}{2N})^d)^{\otimes w}$. Note that $\theta((\text{RZ}(\frac{-\pi}{2N})^d)^{\otimes w} (\text{RZ}(\frac{-\pi}{2N})^d)^{\otimes w}) = w d \theta(\text{RZ}(\frac{-\pi}{N})) = N \frac{\pi}{N} = \pi$, so in theory, each shape w, d gives perfect discrimination. As X, \sqrt{X}, RZ are native gates in IBMQ Brisbane this part of the circuit is implemented exactly as stated. To define the discriminator $|\psi\rangle$, we solve

$$\langle \psi | \left(\text{RZ}(\frac{-\pi}{N})^d \right)^{\otimes w} |\psi\rangle = 0. \quad (17)$$

We find that the input state can be taken as the GHZ state $|\psi\rangle = \frac{1}{\sqrt{2}}(|0\dots 0\rangle + |1\dots 1\rangle)$, which can be implemented by Hadamard gate followed by cascade of control-X gates. We let the IBM transpiler to optimize the input state circuit with the optimization level set to 3.

We distinguish two situations depending on the value of Φ . If $\Phi = \Phi_U$, then the input state $|\psi\rangle$ evolved under U_* is equal to $|\psi_{-i}\rangle = \frac{1}{\sqrt{2}}(|0\dots 0\rangle - i|1\dots 1\rangle)$. For $\Phi = \Phi_V$ we get after the evolution V_* that $|\psi_i\rangle = \frac{1}{\sqrt{2}}(|0\dots 0\rangle + i|1\dots 1\rangle)$. At the measurement stage we implement $\text{RZ}(\pi/2)$ on the first qubit followed by parallel application of Hadamard gates $H^{\otimes w}$. Each qubit is then measured in the Z -basis. We let the IBM transpiler to optimize the measurement circuit with the optimization level set to 3. At the measurement stage, after applying $\text{RZ}(\pi/2)$ and $H^{\otimes w}$ we get

$$H^{\otimes w} (\text{RZ}(\pi/2) \otimes \mathbb{1}) |\psi_{\mp i}\rangle = |+\dots+\rangle \pm |-\dots-\rangle, \quad (18)$$

where we used the notation of plus/minus states $|+\rangle = H|0\rangle, |-\rangle = H|1\rangle$. Observe that if (b_1, \dots, b_w) is a bit string we received from measuring $|+\dots+\rangle \pm |-\dots-\rangle$, then in theory, $\Phi = \Phi_U$ if and only if $b_1 \oplus \dots \oplus b_w \equiv 0$. Similarly, $\Phi = \Phi_V$ if and only if $b_1 \oplus \dots \oplus b_w \equiv 1$.

6.2. Results. From relatively small number of copies ($N = 4, 16, 32$) of unitary channels to be discriminated, the experiments involving purely sequential schemes are preferable (see Fig. 10). We observe that the use of entangling gates on real quantum devices introduces a higher error overhead than the decoherence effects arising from increased gate depth in sequential protocols. For an increasing number of copies ($N = 64, 96, 1024$) of unitary channels, we can observe the advantage of usage sequentially-paralleled schemes to achieve more precise results (see Fig. 11). The results consistently show that after some threshold of gate composition, the existing decoherence or accumulative calibration imperfections gives higher error rates than the error rates used to create an entangled state.

6.3. Discussion. In the experiment with $N = 1024$ copies of black-box we obtained totally random results for all schemes considered (see Fig. 11)(c)). Sequential scheme required too much gate composition while parallel one required creating too big GHZ state. Both circuits introduced too much errors to obtain any notable results. The final question that we can ask is if we can do better than that by exploring *suboptimal* circuits. A simple idea goes as follow. We make independent sequential experiments on each of w qubits. For each, we compose d quantum circuits and do independent measurements that indicate which black-box is preferable. As $\theta(V^\dagger U) = \frac{\pi}{N}$ for each qubit we get the maximum angle spread of $\theta = \frac{\pi}{N} d = \frac{\pi}{w} < \pi$. Hence, the protocol is suboptimal. The probability of successful discrimination can be boosted by using majority voting on the results collected from the

quantum computer. Lets assume we collected k times label 0 indicating Φ_U and $w - k$ times label 1 standing for Φ_V . If $k > w - k$ we guess that $\Phi = \Phi_U$ (and for $k < w - k$ we guess $\Phi = \Phi_V$). In the case $k = w - k$ we take random guess.

We applied the following suboptimal procedure for $N = 1024$. We used $w = 32$ qubits in one experiment and on each of them, we composed $d = 32$ times the operation Φ . According to Fig. 10 we should expect around 90% accuracy for each qubit. In combine we received $p_{\text{succ}} = 0.56765$ that is better than any optimal scheme. Similarly, we did the experiment for $N = 96$ and $w = 3, d = 32$ resulting in $p_{\text{succ}} = 0.74685$, which is better result than indicated by Fig. 11)(b).

Can we say that suboptimal circuits are in favor for unitary channel discrimination? The answer is not straightforward. For example, if $N = 64$ then the best result from Fig. 11)(a) is slightly better than suboptimal procedure presented above even in the absence of the noise, $p_{\text{succ}} = 0.85295$.

7. CONCLUSION

In this work, we have studied the discrimination of two quantum unitary channels and benchmarked various schemes for perfect discrimination between them. The benchmarks have been performed using the IBM Brisbane quantum device. As the first example, we have chosen the discrimination task between the identity operation and the $\text{RZ}(\phi)$ gate with no processing between them. To optimize circuit performance for this discrimination task, we also evaluated different quantum circuit transpilation approaches on 6- and 11-qubit subsystems, comparing the circuit implementation with CNOT and ECR gates and the impact of manual qubit mapping. Although fixed qubit mapping did not significantly improve accuracy in the smaller 6-qubit system (see Table 1), topology-aware circuit design combined with fixed mapping yielded substantial gains on the 11-qubit system when using XOR-based measurements, underscoring the importance of hardware-aware optimization for larger circuits (see Table 2). In this experiment, we find the trend that deeper circuit architectures, which minimize entanglement overhead while preserving discrimination power, are significantly more resilient to hardware noise (see Fig. 7). Our preliminary research suggested the claim that algorithm designers should prioritize depth over width in circuit construction if possible. In the second example, we have considered the discrimination between unitaries $U = \sqrt{X}\text{RZ}(\frac{-\pi}{2N})\sqrt{X}$ and Φ_V for $V = \sqrt{X}\text{RZ}(\frac{\pi}{2N})\sqrt{X}$ with processing being composition of X and \sqrt{X} gates. There, we have observed the advantage of usage sequentially-paralleled schemes to achieve more precise results. The results consistently show that after some threshold of gate composition, the existing decoherence or accumulative calibration imperfections gives higher error rates than the error rates used to create an entangled state.

Circuit geometries beyond square layouts may offer a more accurate reflection of the capabilities of the device. This result can be applied to various black-box tasks with many copies, such as quantum phase estimation [50]. In that case, discrimination schemes that are theoretically suboptimal achieve good experimental performance [51].

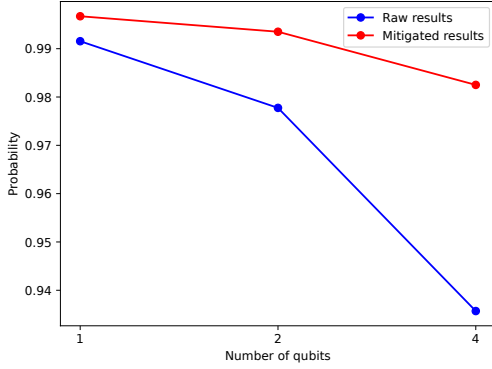
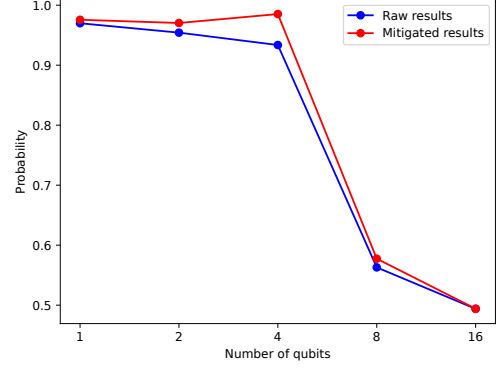
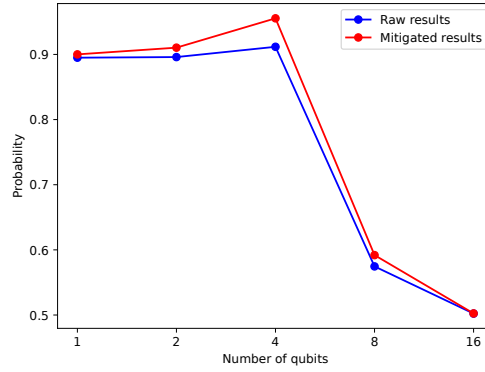
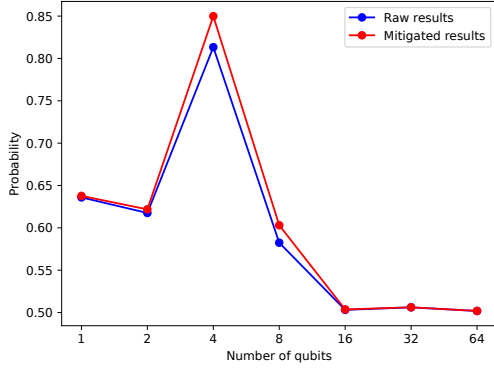
(a) Hybrid scheme for $N = 4$.(b) Hybrid scheme for $N = 16$.(c) Hybrid scheme for $N = 32$.

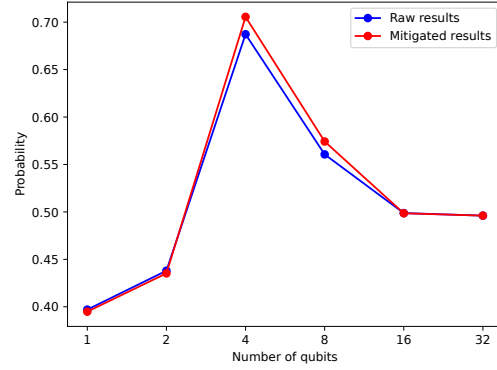
FIGURE 10. Probability of successful discrimination between the unitary operator $U = \sqrt{X}RZ(\frac{\pi}{2N})\sqrt{X}$ and $V = \sqrt{X}RZ(\frac{\pi}{2N})\sqrt{X}$, where N is number of copies of unknown unitary as a function of the width of hybrid rectangular scheme using the short measurement. The blue line corresponds to the results obtained directly from IBM Q processor Brisbane, while the red line represents the results after error mitigation using MThree package [48, 49]. Figure (a) illustrates the performance of hybrid schemes with 4 copies in total, Figure (b) corresponds to hybrid schemes with 16 copies in total, and Figure (c) corresponds to hybrid schemes with 32 copies in total. Each circuit was executed with 10,000 shots per gate.

DATA AVAILABILITY STATEMENT

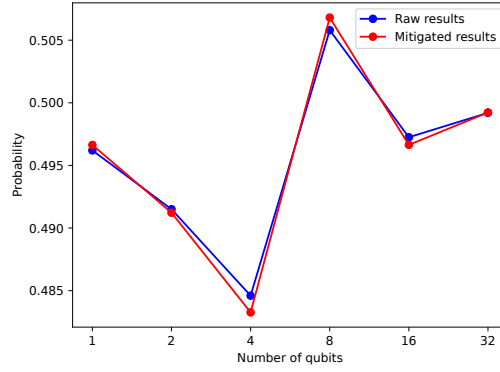
The data that support the findings of this study are openly available in Github repository at https://github.com/Dotnester/experimental_study_of_multiple_shot_channel_discrimination and on Zenodo [52].



(a) Hybrid scheme for $N = 64$.



(b) Hybrid scheme for $N = 96$.



(c) Hybrid scheme for $N = 1024$.

FIGURE 11. Probability of successful discrimination between the unitary operator $U = \sqrt{X}RZ(\frac{\pi}{2N})\sqrt{X}$ and $V = \sqrt{X}RZ(\frac{\pi}{2N})\sqrt{X}$, where N is number of copies of unknown unitary as a function of the width of hybrid rectangular scheme using the short measurement. The blue line corresponds to the results obtained directly from IBM Q processor Brisbane, while the red line represents the results after error mitigation using MThree package [48, 49]. Figure (a) illustrates the performance of hybrid schemes with 64 copies in total, Figure (b) corresponds to hybrid schemes with 96 copies in total, and Figure (c) corresponds to hybrid schemes with 1024 copies in total. Each circuit was executed with 10,000 shots per gate.

ACKNOWLEDGEMENTS

It is a pleasure to thank Łukasz Pawela for numerous discussions concerning experiments on IBM quantum devices.

AB is supported by Grant of SGS No. SP2025/049, VŠB - Technical University of Ostrava, Czech Republic. JH is supported by the Ministry of Education, Youth and Sports of the Czech Republic through the e-INFRA CZ (ID:90254), with the financial support by Grant of SGS No. SP2025/049, VŠB - Technical University of Ostrava, Czech Republic. TB is supported by Grant of SGS No. SP2025/049, VŠB - Technical University of Ostrava, Czech Republic. PL is supported by the Ministry of Education, Youth and Sports of the Czech Republic through the e-INFRA CZ (ID:90254), with the financial support of the European Union under the REFRESH – Research Excellence For REgionSustainability and High-tech Industries project number CZ.10.03.01/00/22_003/0000048 via the Operational Programme Just Transition. RK is supported by the European Union under the REFRESH – Research Excellence For REgionSustainability and High-tech Industries project number CZ.10.03.01/00/22_003/0000048 via the Operational Programme Just Transition.

REFERENCES

- [1] Jens Eisert, Dominik Hangleiter, Nathan Walk, Ingo Roth, Damian Markham, Rhea Parekh, Ulysse Chabaud, and Elham Kashefi. Quantum certification and benchmarking. *Nature Reviews Physics*, 2(7):382–390, 2020.
- [2] David C McKay, Ian Hincks, Emily J Pritchett, Malcolm Carroll, Luke CG Govia, and Seth T Merkel. Benchmarking quantum processor performance at scale. *arXiv preprint arXiv:2311.05933*, 2023.
- [3] Timothy Proctor, Kevin Young, Andrew D Baczewski, and Robin Blume-Kohout. Benchmarking quantum computers. *Nature Reviews Physics*, pages 1–14, 2025.
- [4] Konrad Jałowiecki, Paulina Lewandowska, and Łukasz Pawela. PyQBench: A Python library for benchmarking gate-based quantum computers. *SoftwareX*, 24:101558, 2023.
- [5] Carl W Helstrom. Quantum detection and estimation theory. *Journal of Statistical Physics*, 1:231–252, 1969.
- [6] John Watrous. *The theory of quantum information*. Cambridge university press, 2018.
- [7] Kornikar Sen, Saronath Halder, and Ujjwal Sen. Incompatibility of local measurements providing an advantage in local quantum state discrimination. *Physical Review A*, 109(1):012415, 2024.
- [8] Somshubhro Bandyopadhyay, Saronath Halder, and Michael Nathanson. Optimal resource states for local state discrimination. *Physical Review A*, 97(2):022314, 2018.
- [9] J Calsamiglia, JI De Vicente, Ramon Muñoz-Tapia, and E Bagan. Local discrimination of mixed states. *Physical Review Letters*, 105(8):080504, 2010.
- [10] János A Bergou, Ulrike Herzog, and Mark Hillery. 11 discrimination of quantum states. *Quantum state estimation*, pages 417–465, 2004.
- [11] Daowen Qiu. Minimum-error discrimination between mixed quantum states. *Physical Review A—Atomic, Molecular, and Optical Physics*, 77(1):012328, 2008.
- [12] John Watrous. Simpler semidefinite programs for completely bounded norms. *Chicago Journal of Theoretical Computer Science*, 8:1–19, 2013.
- [13] Giuliano Benenti and Giuliano Strini. Computing the distance between quantum channels: usefulness of the fano representation. *Journal of Physics B: Atomic, Molecular and Optical Physics*, 43(21):215508, 2010.
- [14] Motakuri V Ramana. An exact duality theory for semidefinite programming and its complexity implications. *Mathematical Programming*, 77:129–162, 1997.

- [15] Piotr Gawron, Dariusz Kurzyk, and Łukasz Paweła. QuantumInformation.jl—a julia package for numerical computation in quantum information theory. *PLOS ONE*, 13(12):e0209358, dec 2018.
- [16] Mário Ziman and Michal Sedlák. Single-shot discrimination of quantum unitary processes. *Journal of Modern Optics*, 57(3):253–259, 2010.
- [17] Łukasz Paweła, Piotr Gawron, Jarosław Adam Miszczak, Zbigniew Puchała, Karol Życzkowski, Paulina Lewandowska, and Ryszard Kukulski. Numerical shadow. The web resource at <https://numericalshadow.org/>. Accessed on 2020-05-25.
- [18] Michal Sedlák and Mário Ziman. Optimal single-shot strategies for discrimination of quantum measurements. *Physical Review A*, 90(5):052312, 2014.
- [19] Aleksandra Krawiec, Łukasz Paweła, and Zbigniew Puchała. Discrimination and certification of unknown quantum measurements. *Quantum*, 8:1269, 2024.
- [20] Zbigniew Puchała, Łukasz Paweła, Aleksandra Krawiec, and Ryszard Kukulski. Strategies for optimal single-shot discrimination of quantum measurements. *Physical Review A*, 98(4):042103, 2018.
- [21] Aleksandra Krawiec, Łukasz Paweła, and Zbigniew Puchała. Discrimination of povms with rank-one effects. *Quantum Information Processing*, 19:1–12, 2020.
- [22] Zhengfeng Ji, Yuan Feng, Runyao Duan, and Mingsheng Ying. Identification and distance measures of measurement apparatus. *Physical Review Letters*, 96(20):200401, 2006.
- [23] Tian-Qing Cao, Fei Gao, Zhi-Chao Zhang, Ying-Hui Yang, and Qiao-Yan Wen. Perfect discrimination of projective measurements with the rank of all projectors being one. *Quantum Information Processing*, 14(7):2645–2656, 2015.
- [24] Ognjan Oreshkov, Fabio Costa, and Časlav Brukner. Quantum correlations with no causal order. *Nature Communications*, 3(1):1–8, 2012.
- [25] Mateus Araújo, Cyril Branciard, Fabio Costa, Adrien Feix, Christina Giarmatzi, and Časlav Brukner. Witnessing causal nonseparability. *New Journal of Physics*, 17(10):102001, 2015.
- [26] Paulina Lewandowska, Łukasz Paweła, and Zbigniew Puchała. Strategies for single-shot discrimination of process matrices. *Scientific Reports*, 13(1):3046, 2023.
- [27] Farzin Salek, Masahito Hayashi, and Andreas Winter. Usefulness of adaptive strategies in asymptotic quantum channel discrimination. *Physical Review A*, 105(2):022419, 2022.
- [28] Jessica Bavaresco, Mio Murao, and Marco Túlio Quintino. Strict hierarchy between parallel, sequential, and indefinite-causal-order strategies for channel discrimination. *Physical Review Letters*, 127(20):200504, 2021.
- [29] Jessica Bavaresco, Mio Murao, and Marco Túlio Quintino. Unitary channel discrimination beyond group structures: Advantages of sequential and indefinite-causal-order strategies. *Journal of Mathematical Physics*, 63(4), 2022.
- [30] Runyao Duan, Cheng Guo, Chi-Kwong Li, and Yinan Li. Parallel distinguishability of quantum operations. In *2016 IEEE International Symposium on Information Theory (ISIT)*, pages 2259–2263. IEEE, 2016.
- [31] Giulio Chiribella, Giacomo M D’Ariano, and Paolo Perinotti. Memory effects in quantum channel discrimination. *Physical Review Letters*, 101(18):180501, 2008.
- [32] Runyao Duan, Yuan Feng, and Mingsheng Ying. Entanglement is not necessary for perfect discrimination between unitary operations. *Physical Review Letters*, 98(10):100503, 2007.
- [33] Aram W Harrow, Avinandan Hassidim, Debbie W Leung, and John Watrous. Adaptive versus non-adaptive strategies for quantum channel discrimination. *Physical Review A*, 81(3):032339, 2010.
- [34] Masahito Hayashi. Discrimination of two channels by adaptive methods and its application to quantum system. *IEEE Transactions on Information Theory*, 55(8):3807–3820, 2009.
- [35] Guoming Wang and Mingsheng Ying. Unambiguous discrimination among quantum operations. *Physical Review A*, 73(4):042301, 2006.
- [36] Runyao Duan, Yuan Feng, and Mingsheng Ying. Perfect distinguishability of quantum operations. *Physical Review Letters*, 103(21):210501, 2009.
- [37] Zbigniew Puchała, Łukasz Paweła, Aleksandra Krawiec, Ryszard Kukulski, and Michał Oszmaniec. Multiple-shot and unambiguous discrimination of von neumann measurements. *Quantum*, 5:425, 2021.

- [38] Shusen Liu, Yinan Li, and Runyao Duan. Distinguishing unitary gates on the ibm quantum processor. *Science China Information Sciences*, 62:1–7, 2019.
- [39] Felix Hausdorff. Der wertvorrat einer bilinearform. *Mathematische Zeitschrift*, 3:314–316, 1919.
- [40] Otto Toeplitz. Das algebraische analogon zu einem satze von fejér. *Mathematische Zeitschrift*, 2:187–197, 1918.
- [41] Alexander S. Holevo. Statistical decision theory for quantum systems. *Journal of Multivariate Analysis*, 3(4):337–394, 1973.
- [42] J. Watrous. *The Theory of Quantum Information*. Cambridge University Press, 2018.
- [43] John Watrous. Channel distinguishability and the completely bounded trace norm. Technical Report CS 766 / QIC 820 Lecture 20, University of Waterloo, November 2011. Available at <https://johnwatrous.com/wp-content/uploads/TQI-notes.20.pdf>.
- [44] Antonio Acín. Statistical distinguishability between unitary operations. *Physical Review Letters*, 87(17):177901, 2001.
- [45] G Mauro D’Ariano, Paoloplacido Lo Presti, and Matteo GA Paris. Using entanglement improves the precision of quantum measurements. *Physical Review Letters*, 87(27):270404, 2001.
- [46] Zachary Eldredge, Michael Foss-Feig, Jonathan A Gross, Steven L Rolston, and Alexey V Gorshkov. Optimal and secure measurement protocols for quantum sensor networks. *Physical Review A*, 97(4):042337, 2018.
- [47] The web resource at <https://docs.quantum.ibm.com/guides/processor-types>. Accessed on 2025-05-18.
- [48] <https://qiskit.org/documentation/partners/mthree/stubs/mthree.M3Mitigation.html> The web resource at <https://qiskit.org/documentation/partners/mthree/stubs/mthree.M3Mitigation.html>. Accessed on 2025-05-18.
- [49] Paul D Nation, Hwajung Kang, Neereja Sundaresan, and Jay M Gambetta. Scalable mitigation of measurement errors on quantum computers. *PRX Quantum*, 2(4):040326, 2021.
- [50] Uwe Dorner, Rafal Demkowicz-Dobrzanski, Brian J Smith, Jeff S Lundeen, Wojciech Wasilewski, Konrad Banaszek, and Ian A Walmsley. Optimal quantum phase estimation. *Physical Review Letters*, 102(4):040403, 2009.
- [51] Krysta M Svore, Matthew B Hastings, and Michael Freedman. Faster phase estimation. *Quantum Information & Computation*, 14(3-4):306–328, 2014.
- [52] Adam Bílek, Jan Hlisnikovský, Tomáš Bezděk, Ryszard Kukulski, and Paulina Lewandowska. Zenodo: Experimental study of multiple-shot unitary channels discrimination using the IBM Q computers, <https://doi.org/10.5281/zenodo.15464711>, May 2025.